ALMA MEMO 389

Radio Interferometer Array Point Spread Functions

I. Theory and Statistics

David Woody[1]

Abstract— **This paper relates the optical definition of the PSF to radio interferometer arrays. The statistical properties of the PSF including the effect of missing UV data are derived as a function of the number of antennas and array magnification, defined as the ratio of the primary beam width from an individual element to the synthesized beam width. The effect of earth rotation synthesis on the PSF is also calculated and the merits of various configuration strategies are discussed in terms of their PSFs.**

The concept of a pseudo-random array is introduced as an array whose large-scale average distribution matches an idealized continuous antenna distribution. The small-scale difference between the actual discrete distribution and the idealized continuous distribution produces far sidelobes in the PSF. It is shown that the statistical distribution of the sidelobes, s, of pseudo-random arrays of N antennas with sparse UV coverage is given by $P(s) = N\exp(-Ns)$. The average sidelobe is 1/N and the standard deviation is also 1/N. Note that the single antenna measurements are included in the formulation of the PSF used in this work. The expected peak sidelobe for a pseudo-random array with a magnification mag is $s_{max} \approx 2\ln(mag)/N$ and it is predicted that optimization can reduce the peak sidelobe to $s_{max,opt} \approx \left(2\ln(mag) - \ln(N)\right)/N$. Pseudo-random arrays provide a benchmark against which proposed configurations can be compared.

I. INTRODUCTION

The point spread function, PSF, is very useful and convenient for evaluating the performance of an imaging system [1]. The PSF is the response of an imaging system to a point source and the "raw" image produced by the system is the true image convolved with the PSF. Thus the PSF is a good measure of the errors and artifacts that will appear in the raw image.

The PSF functions for optical instruments are usually of sufficient quality that the raw images can be published with little or no image processing. Radio interferometers do not directly measure the image, but must reconstruct the image from limited visibility measurements. The response to a point source or PSF can still be calculated, but unfortunately most existing interferometers have relatively poor PSFs and useful images are produced only after applying non-linear deconvolution imaging techniques such as CLEAN and MEM [2]. The ability of the imaging algorithms to produce faithful representations of the true sky brightness distribution in the presence of noise is limited by both the near and far sidelobes of the PSF. The quality of the PSF in typical radio interferometers is indicated by the fact that it is often called the "dirty beam". Respectable PSFs can be produced by interferometers with a large number of antennas, such as ALMA which will have ~64 antennas.

Most of the imaging quality and UV distribution parameters can be identified with features in the PSF. The dynamic range between a strong unresolved source and distant noise in the "raw" or "dirty" image is determined by the far sidelobes of the PSF. The near sidelobes determine the fidelity for imaging extended objects. Although algorithms such as CLEAN or MEM can dramatically decrease the effect of the sidelobes, their ability of accomplish this in the presence of noise and imperfect knowledge of the phase and amplitude of the aperture illumination is limited. The PSF measures the magnitude of the defects that must be corrected by any imaging algorithm and arrays with smaller PSF sidelobes should produce more accurate images. Many millimeter and sub-millimeter observations will be noise limited and an array with a PSF that has sidelobes less than the signal to noise on the strongest source will be able to use the raw image directly.

The task of determining the best array configurations for ALMA involves many conflicting requirements ranging from imaging performance to geographical limits on where antenna can be economically placed. Although complex imaging simulations can be used to evaluate many aspects of the imaging performance, it is necessary to have a quick and easy method for determining the effect of perturbing the configurations. A simple evaluation metric is very useful during both the initial design phase when many different configurations need to be characterized and during the detailed design phase when practical considerations may require moving some of the pad locations. The PSF serves this purpose very well.

The general discussion of the merits of ring type arrays with their more uniform UV coverage versus uniform or centrally condensed arrays with more Gaussian UV coverage can be carried out quantitatively in terms of the sidelobe distribution. This paper gives a quantitative basis for Holdaway's discussion of the tradeoffs ring-like and filled array configurations [3].

The next section develops the basic foundation for calculating the PSF for a radio interferometer array while adhering closely to the optical terminology. The formulations presented in this section are well known, but it is useful to explicitly restate them here for use in later sections. Section III evaluates the near sidelobes produced by various large-scale antenna distributions. Section IV introduces the pseudo-random array whose large-scale distribution matches an idealized continuous distribution but has small-scale deviations. The effect of these small-scale deviations is measured by the difference between the actual PSF and the PSF of the idealized distribution. The statistics of this difference PSF are derived in this section, including the expected magnitude of the largest sidelobes. Various other considerations, such as earth rotation synthesis and the implications of obtaining nearly complete UV coverage, are discussed in section V. The implications of these results and conclusions are discussed in section VI.

A second paper titled "Radio Interferometer Array Point Spread Functions II. Evaluation and Optimization" presents the PSF for several sample configurations and optimized versions of these configurations. The paper also shows different methods for presenting the PSF that make it easy to discern the differences between various configurations and demonstrates the validity of the statistical distributions derived in this paper.

II.   INTERFEROMETER POINT SPREAD FUNCTION

The definition of the PSF for interferometers should be consistent with the PSF defined for optical telescopes to allow similar interpretation of the resulting images.

A.   Optical PSF

The PSF is widely used for characterizing the performance of optical telescopes. The PSF given for radio interferometers should be consistent with this usage. The PSF for optical telescopes is the image intensity distribution of the focal plane image of a plane wave incident on the aperture. This intensity is the square of the field magnitude in the focal plane which is in turn the Fourier transform of the complex field (amplitude and phase) across the aperture.

An array of N small apertures produces a focal plane voltage field that can be written as the sum of the focal plane fields from the individual apertures,

$$U_{PSF}(\vec{p}) = \frac{1}{N}\sum_{n=1}^{N} U_n(\vec{p})\exp\left(-ik\,\vec{p}\cdot\vec{r}_n\right). \tag{1}$$

$\vec{p}$ is the position vector on the sky and $U_n(\vec{p})$ is the voltage beam pattern for aperture k. $\vec{r}_n$ is the location vector for the center of the n_{th} aperture. The PSF for an array of N identical apertures is then given by

$$PSF(\vec{p}) = \left|U_{PSF}(\vec{p})\right|^2$$
$$= \frac{1}{N^2}\sum_{m=1}^{N}\sum_{n=1}^{N} B(\vec{p})\exp\left(-ik\,\vec{p}\cdot(\vec{r}_m-\vec{r}_n)\right)^. \tag{2}$$

$B(\vec{p}) = \left|U(\vec{p})\right|^2$ is the primary beam power pattern for a single aperture in the array.

The Wiener-Khintchine relations can be used to write the PSF as the Fourier transform of the autocorrelation of the total aperture field pattern. This autocorrelation is called the Optical Transfer Function, OTF, in optical systems [4] or the UV coverage for radio interferometers. The OTF for an array is given by

$$OTF(\vec{u}) = \frac{1}{N^2}\sum_{m=1}^{N}\sum_{n=1}^{N} A(\vec{u}-\vec{b}_{m,n}) , \tag{3}$$

where $\vec{u}$ is the vector position in the UV plane and $\vec{b}_{m,n}$ is the baseline vector connecting the m_{th} and n_{th} elements. $A(\vec{u})$ is the autocorrelation of the field pattern, or OTF, for a single element in the array. The double summation over both indices explicitly includes the single aperture measurements and ensures that the PSF is positive everywhere.

B.   Radio interferometer formulation

Radio interferometers measure the visibility or complex product of the voltages received by pairs of antennas and do not directly produce images in a focal plane. The measured visibility is the Fourier transform of the sky brightness times $B(\vec{p})$ [5]. The same PSF formulation given in equ. 1 can be arrived at for a radio interferometer by calculating the cross coupling or orthogonality of the measurements of two point sources. The measurement vector, $M(\vec{p})$, is the set of measured visibilities plus the single antenna power measurements. The l_{th} component corresponding to measuring the visibility on baseline $\vec{b}_l = (\vec{r}_m - \vec{r}_n)$ of a point source at $\vec{p}$ is

$$M(\vec{p})_l = B(\vec{p})\exp\left(-ik\,\vec{p}\cdot\vec{b}_l\right). \tag{4}$$

A snapshot with an N element array will produce N^2 components when the Hermitian conjugates and single element measurements are included. The cross coupling between measurements of a point source at $\vec{p}$ and a neighboring point at $\vec{p}+\Delta p$ is given by the dot product of the measurement vectors

$$\vec{M}(\vec{p}+\Delta p)\bullet\vec{M}(\vec{p})^* = \frac{1}{N^2}\sum_{l=1}^{N^2} B(\vec{p}+\Delta\vec{p})B(\vec{p})\exp\left[-ik\,\Delta\vec{p}\cdot\vec{b}_l\right]. \tag{5}$$

A cross coupling of zero means that two point sources as $\vec{p}$ and $\vec{p}+\Delta\vec{p}$ can be uniquely measured with no confusion, while a large cross coupling means that the sources are

ALMA MEMO 389

difficult to distinguished. Equ. 5 reduces to equ. 2 when $\vec{p}=0$, i.e. a point source at field center.

Equ. 5 can be used to define the PSF for a point source at a point $\vec{p}$ away from the field center as a function of the offset distance $\Delta\vec{p}$ to a neighboring point,

$$PSF(\vec{p},\Delta\vec{p}) = \vec{M}(\vec{p}+\Delta\vec{p}) \bullet \vec{M}(\vec{p}) . \qquad (6)$$

There will be a family of PSFs, a different PSF for each $\vec{p}$. The maximum sidelobe as a function of distance from the point source is of interest in evaluating an array's imaging performance and is given by the upper envelope of the family of PSFs. A single plot can show this maximum for all point source positions by using a modified primary beam pattern

$$B'(\Delta\vec{p}) = \max[B(\vec{p}+\Delta\vec{p})B(\vec{p}), \vec{p}] . \qquad (7)$$

The max function returns the maximum of the product as a function of $\vec{p}$. The modified beam pattern is a wider version of the single antenna primary beam. A Gaussian primary beam remains Gaussian but becomes $\sqrt{2}$ wider. The worst case PSF' is given by

$$PSF'(\Delta\vec{p}) = \frac{1}{N^2}\sum_{l=1}^{N^2} B'(\Delta\vec{p})\exp(-ik\Delta\vec{p}\cdot\vec{b}_l) . \qquad (8)$$

The corresponding OTF for a single element, $A'(\vec{b})$, is the Fourier transform of $B'(\vec{p})$.

Data weighting or additional measurements can be incorporated into this formulation of the PSF. Added data from other configurations or arrays just increases the number of vector components. Component coefficients can be used in equ. 8 to account for different noise levels in each visibility or to improve the sidelobes. This approach can also be used to evaluate an array's ability to distinguish or identify sources that are not point like by appropriate formulation of the measurement vectors.

III. LARGE-SCALE DISTRIBUTION

The central beam and near sidelobes for an array consisting of a large number of antennas will be determined by the large-scale distribution of antennas. These features of the PSF can be investigated by evaluating the PSF for various candidate continuous functions. A sample of continuous antenna distributions is shown in fig. 1. The autocorrelations corresponding to the UV coverage of the distributions are shown in fig. 2 while their PSF's are presented in fig. 3. The distributions were scaled to produce beams with the same FWHM.

As expected, the size of the near sidelobes decreases as the antenna distributions become smoother and more bell shaped. The tradeoff between sidelobe level and maximum baseline length for a given resolution is also apparent from these figures. The thin ring array requires the shortest maximum baseline and produces the most uniform UV coverage, but at the cost of sidelobes as large as 16%. The uniform antenna
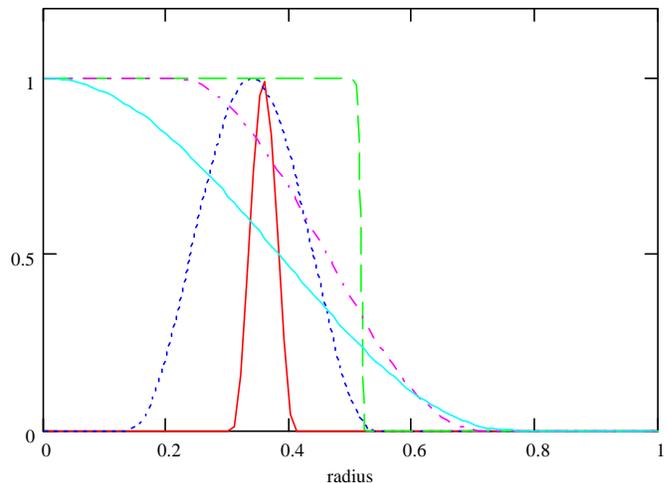

Fig. 1. Radial slices through five different cylindrically symmetric large-scale antenna distributions.
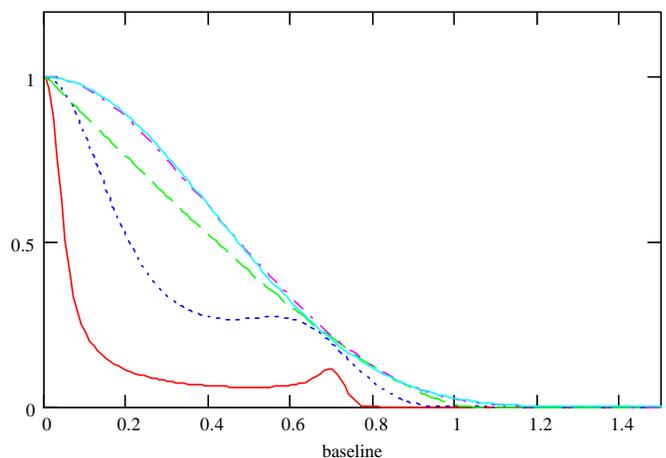

Fig. 2. The UV distribution or OTF for the five distributions shown in fig. 1. The line style and colors are the same as for fig. 1.
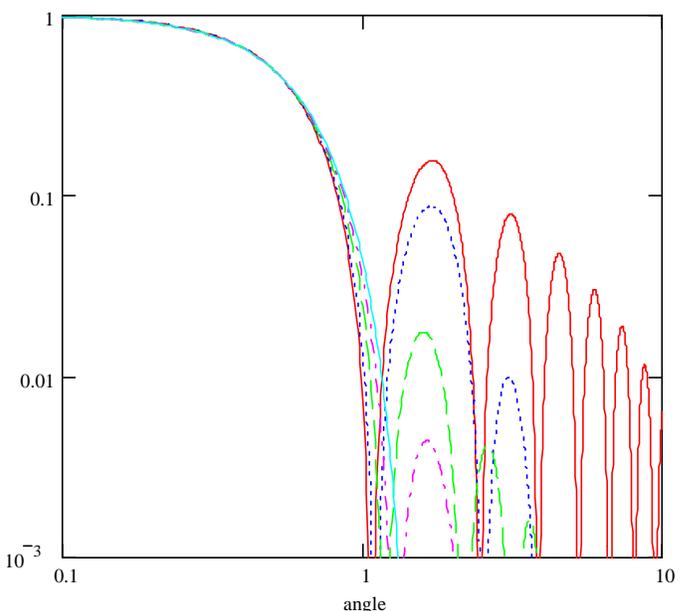

Fig. 3. The PSF for each of the five antenna distributions shown in fig. 1.

distribution has a first sidelobe of ~1.6%. The $\cos^2$ bell shaped distribution has no sidelobes above 0.1%. The basic large-scale distribution can be selected based upon the acceptable sidelobe level, desired resolution, and available real estate.

IV. SMALL-SCALE DISTRIBUTION AND STATISTICS OF THE DIFFERENCE PSF

Matching a large-scale distribution with a finite number of antennas will necessarily leave small-scale deviations from the target distribution

$$D(\bar{u}) = S(\bar{u}) - I(\bar{u}) . \tag{9}$$

$S(\bar{u})$ is the actual UV sample distribution or OTF given by equ. 3. $I(\bar{u})$ is the ideal target UV sample distribution.

Fourier transforming the UV functions in equ. 9 gives their corresponding PSFs

$$D(\bar{p}) = S(\bar{p}) - I(\bar{p}) . \tag{10}$$

We will assume that the actual distribution closely matches the large-scale structure of the ideal distribution and hence the error or difference beam is close to zero near the center of the beam and equal to the actual PSF in the far sidelobes. Alternatively, the idealized continuous distribution can be define as the actual distribution smoothed on a suitable large-scale. Note that single dish measurements from the N antennas as well as the Hermitian conjugate UV samples are included in this formulation and the actual PSF function from an array as well as the ideal PSF derived from a positive real aperture field distribution is positive and real.

A. Average sidelobes

The integral of the actual far sidelobes is closely given by the integral of the difference beam. This in turn is equal to the difference between the idealized distribution and the actual UV sampling at $\bar{u} = 0$,

$$\iint D(\bar{p})d\bar{p} = S(0) - I(0)$$
$$= \frac{1}{N} A(0) - I(0) \tag{11}$$

This uses equ. 3 noting that N single antenna measurements contribute to $S(0)$. $I(\bar{u})$ and $A(\bar{u})$ are normalized to have an integrated volume of unity and hence $I(0)$ and $A(0)$ are inversely proportional to the area encompassing the array and the area of a single telescope respectively. The area encompassing the array must necessarily be significantly larger than the total antenna collecting area and the first term in the second line of equ. 11 will dominate.

The average of the PSF sidelobes is obtained by dividing the integrated sidelobes by the area of the primary beam, which is equal to $A(0)$, conveniently yielding

$$\overline{D(\bar{p})} \approx \frac{1}{N} . \tag{12}$$

The actual average for the PSF sidelobes can be altered by varying the number of single antenna measurements contributing to the $\bar{u} = 0$ sample. Kogan shows that in the absence of single antenna measurements the average sidelobe is zero and the peak negative sidelobes have amplitude $\leq 1/(n-1)$ [6].

B. Missing UV samples and standard deviation of sidelobes

It should be possible to match the ideal large-scale distribution reasonably well in regions where the UV samples are separated by less than the antenna diameter d, especially if the ideal UV distribution is derived from the autocorrelation of a feasible antenna distribution. But for the larger configurations there will be regions where the UV samples are separated by more than d and the contrast between the areas where there are no samples and the discrete samples will produce relatively large deviations from the ideal distribution.

The difference distribution, $D(\bar{u})$, becomes a two valued function in the regions of sparse coverage if we approximate the antenna OTF, $A(\bar{u})$, by a top hat of height $A(0)$ and diameter $d' = 2\sqrt{\pi A(0)}$. The two values of $D(\bar{u})$ are $-I(\bar{u})$ and $(A(0)/N^2 - I(\bar{u}))$. The assumption that the actual and ideal distributions match on the large scale implies that the UV samples cover a fraction of the UV plane given by

$$f(\bar{u}) = I(\bar{u}) \frac{N^2}{A(0)} . \tag{13}$$

The mean square value of a function that takes on the value $(A(0)/N^2 - I(\bar{u}))$ over a fraction $f(\bar{u})$ of the area and the value $-I(\bar{u})$ over the rest of the area is

$$\overline{D^2(\bar{u})} = f(\bar{u}) \frac{A^2(0)}{N^4} - 2f(\bar{u}) \frac{A(0)}{N^2} I(\bar{u}) + I^2(\bar{u})$$
$$= I(\bar{u}) \frac{A(0)}{N^2} - I^2(\bar{u}) \tag{14}$$

The second term in the second line is negligible and can be safely ignored. Parseval's theorem tells us the integrated square of the difference PSF is equal to the integrated square of the difference OTF. A lower limit to the integrated square of the difference PSF is obtained by integrating equ. 14 over the regions where fractional coverage, $f(\bar{u})$, is less than one. As with the calculation of the average value of the PSF, the average square of the difference PSF is obtained by dividing by $A(0)$. Hence a lower limit to the standard deviation of the difference PSF is

ALMA MEMO 389

$$\sigma_D \ge \left[\iint_{f(\vec{b}) \le 1} I(\vec{u}) \frac{1}{N^2} d\vec{u} \right]^{1/2} \quad . \tag{15}$$

This reduces to a particularly simple result for very large configurations where $f(\vec{u}) < 1$ over the full UV plane

$$\sigma_D \ge \frac{1}{N} . \tag{16}$$

Using the actual single antenna OTF instead of the assumed top hat function complicates the derivation, but the results shown in equ. 15 and 16 are still valid.

Evaluating equ. 15 for smaller configurations requires knowing the idealized distribution. The standard deviations of the difference PSF for 64 antenna arrays with bell shaped and uniform UV distributions are plotted as a function of the array magnification in fig. 4. The magnification is the ratio of the primary beam to the synthesized beam. The lower limit for the standard deviation for the bell shaped distribution of N antennas increases linearly for magnifications up to ~N and saturates at a value 1/N for magnifications >2N. The uniform UV distribution has complete coverage up to a magnification of ~N and hence no lower limit to the standard deviation of the difference PSF until the magnification exceeds this magnification.

C. Statistical distribution of sidelobe peaks

Any detectable pattern in the antenna distribution will result in noticeable features in the OTF and in the PSF sidelobes. A random antenna distribution that statistically matches the desired ideal distribution is expected to produce the minimum sidelobes over the full primary beam. The full statistical distribution of sidelobes can be calculated for such pseudo-random arrays operating at large magnification, i.e. sparse UV coverage.

Equ. 1 shows that the complex voltage in the image plane is the result of adding N complex numbers or steps of magnitude $E(\vec{p})/N$ with different phases. The phase of the l_{th} complex number for the PSF at $\vec{p}$ is $k\,\vec{r}_l \bullet \vec{p}$. Away from the central peak in the PSF this phase is many turns and each step has an essentially random phase relative to the other N-1 steps. Each point in the PSF is then essentially a 2-D random walk of N steps. The variance of each component of the individual steps is

$$\sigma_{l,x}^2 = \sigma_{l,y}^2 = \left(\frac{E(\vec{p})}{2N} \right)^2 . \tag{17}$$

The variance for the sum of N of these components is

$$\sigma_x^2(\vec{p}) = \sigma_y^2(\vec{p}) = \frac{B(\vec{p})}{4N} . \tag{18}$$
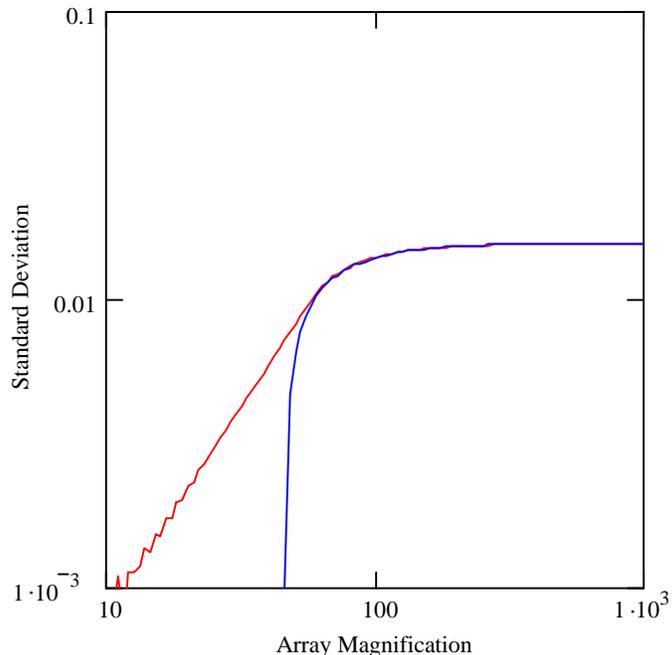

Fig. 4. Approximate lower limit to the standard deviation of the difference PSF as a function of the array magnification for an array of 64 antennas. The red curve is for a bell shaped distribution, while the blue cure is for a uniform UV coverage.

Although the components of each step do not have a Gaussian distribution, the central limit theorem tells us that the distribution of a sum of a large number of steps will approach a Gaussian distribution. Thus we can apply the results obtained for the noise from a cross correlator [7, 8] and the magnitude of the resultant vectors follows a Rayleigh distribution

$$g(v) = 2Nv \exp\!\left(-Nv^2\right). \tag{19}$$

where v is the magnitude of the sum of the N steps of length 1/N and random phase.

The PSF is the magnitude squared of the complex voltage in the image plane. The distribution of the PSF sidelobes, $s = v^2$, is given by

$$g(s) = g(v)\left(\frac{ds}{dv} \right)^{-1} = N \exp\!\left(-Ns\right). \tag{20}$$

This distribution yields the same the sidelobe average and standard deviation derived in equs. 12 and 16 above.

The largest sidelobe in the PSF is an important parameter since it represents the largest imaging artifact that a strong point source can produce. The number of independent sidelobes is roughly given by the square of the ratio of the primary beam to the synthesized beam, i.e. the magnification squared, mag^2. A rough estimate of the largest sidelobe is given by s_{max} such that
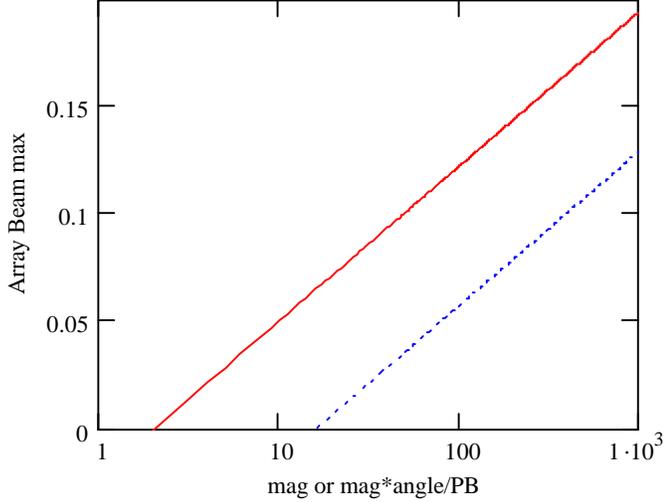
Fig. 5. Plot of the expected peak sidelobe as a function of magnification (or radial distance form beam center) for pseudo-random (solid) and optimized pseudo-random arrays (dotted).

$$\int_{s_{max}}^{\infty} g(s)ds = \exp(-Ns_{max}) = \frac{1}{mag^2}. \tag{21}$$

Hence we expect the peak sidelobe for a pseudo-random array configuration to be

$$s_{max} \approx \frac{2}{N}\ln(mag). \tag{22}$$

This function is plotted fig. 5. The same result can also be derived using the approach employed to determine VLBI false fringe statistics [9] [1].

D. Optimization

The statistical distribution derived in the previous applies to a pseudo-random configuration. There algorithms that can be applied to further improve the PSF. Kogan has developed an algorithm that explicitly minimizes the peak sidelobe over selected areas in the PSF [10] and Boone has developed an algorithm to optimize the match between the UV coverage and a desired large scale distribution [11]. What improvements in the peak sidelobe performance might one expect after trying to optimize the configuration?

There are 2(N-1) degrees of freedom in placing N antennas on a plane. Only a small fraction of these degrees of freedom are used in placing the antennas so as to statistically match the desired large scale distribution in a pseudo-random array. It should be possible to fine tune the antenna positions to decrease the ~N largest peaks. Following the same steps used in equs. 21 and 22 above we arrive at

$$s_{max,opt} \approx \frac{1}{N}\left[2\ln(mag) - \ln(N)\right], \tag{23}$$

and is also plotted in fig. 5.

The sidelobes at different distances from the center of the PSF correspond to different spatial wavenumbers or scale sizes. It should be possible to optimize the near in sidelobes and proceed to optimize the further out sidelobes without grossly worsening the near sidelobes. Because the near sidelobe correspond to effectively smaller magnification, a fully optimized configuration should have a distribution of sidelobe peaks versus distance from the center of the PSF that looks like equ. 22 or 23. This is shown in fig. 5 using the alternate definition of the horizontal scale. Note that this type of distribution of sidelobe peaks is also expected for the unoptimized pseudo-random array simply because the number of independent PSF samples per unit radial distance increases linearly with radius.

V. OTHER CONSIDERATIONS

A. Antennas out of service

The effect of taking an antenna out of service can be conveniently calculated using the formulation of the PSF as the magnitude squared of the voltage in the image plane given in equ. 1. Each antenna contributes a vector step of length 1/N to the voltage sum. The maximum affect on a typical PSF sidelobe of amplitude 1/N of removing the contribution from one antenna is

$$s_{typical} \Rightarrow \left(\frac{1}{\sqrt{N}} \pm \frac{1}{N}\right)^2 \approx \frac{1}{N}\left(1 \pm \frac{2}{\sqrt{N}}\right). \tag{23}$$

Thus the typical sidelobe in a 64 antenna array will change by less than 25% with the removal of one antenna. The sidelobe average increases by 1.6%.

Pseudo-random arrays are particularly resilient to removal of an antenna, since there is no pattern that can be disrupted and all antennas are equally important. The worst possible increment to the maximum sidelobe is

$$s_{max} \Rightarrow \left(\sqrt{\frac{2}{N}\ln(mag)} + \frac{1}{N}\right)^2$$
$$\approx \frac{2}{N}\ln(mag)\left(1 + \sqrt{\frac{2}{N\ln(mag)}}\right). \tag{24}$$

A 64 antenna array operating at a magnification of 100 could have its peak sidelobe increased by as much as 8%.

B. Combining configurations

Many astronomical projects will observe a source for more than a few minutes and may combine several UV data sets. Additional observations add more coverage of the UV plane and can improve the PSF. Adding UV data is a linear operation and the PSF from the different observations are also added linearly. If the sidelobes from the different observations are uncorrelated, the standard deviation of the resultant PSF decreases as the square root of number of configurations.

Extended observational tracks present a special case because the successive UV data sets are highly correlated and the sidelobes do not necessarily decrease. This is especially
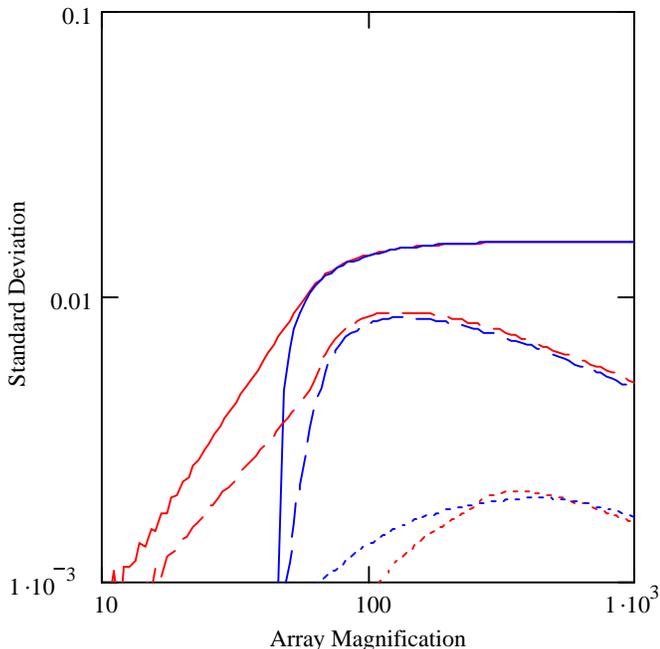
ALMA MEMO 389

Fig. 6. Plot of the lower limit to the standard deviation for bell shaped (red curves) and uniform UV coverage (blue curves) for 64 antenna arrays for snapshot (solid), 6 min (dashed) and 1 hr tracks (dotted).

true for the near sidelobes of the PSF. Long tracks can be handled by scaling the effective number of UV samples and replacing N^2 by $g(\bar{b})N^2$ in equs. 13 and 14, where

$$g(\bar{b}) = 1 + \frac{\theta |\bar{b}|}{d'} \qquad (25)$$

and θ is the earth rotation angle. Equ. 15 becomes

$$\sigma_D^2 \geq \iint\limits_{g(\bar{b})f(\bar{b})\leq 1} I(\bar{b})\frac{1}{g(\bar{b})N^2}d\bar{b} . \qquad (26)$$

Earth rotation can significantly improve the UV coverage and even short tracks will decrease the PSF sidelobes. Fig. 6 shows the improvement than can be obtained with only 6 min and 1 hr tracks. This analysis assumes a circularly symmetric array at the pole observing a polar source. The long baselines sweep over a large area of the UV plane reducing the gaps in the UV coverage and significantly decreasing the standard deviation of the sidelobes. Interestingly, the increased coverage for the higher magnification configurations more than compensates for the reduced snapshot coverage and the sidelobe standard deviation decreases as the configuration size increases. Both the bell shaped and uniform coverage arrays show similar behavior for large magnifications, but there can be significant differences for the small configurations. Because the added coverage is not randomly distributed, the actual decrease in sidelobe standard deviation will be much less than shown in fig. 6.

Earth rotation greatly reduces the standard deviation and peaks of the intermediate and far sidelobes, but does not change the average sidelobe level if the single antenna measurements are acquired continuously during the track. The near sidelobes caused by the large-scale idealized distribution are typically complete elliptical rings and earth rotation will offer only a modest reduction in their peaks. Additionally the UV coverage resulting from earth rotation does not correspond to a pseudo-random array and hence the sidelobes will not necessarily follow the distribution given in equ. 20.

C. Complete coverage

Complete coverage can provide unique images but the accuracy of the images is still limited by the near-in sidelobes caused by the sharp cutoff in the UV coverage at the maximum baseline length and by the far sidelobes caused by the small-scale variations in the UV coverage. The principal advantage of complete coverage is that there are no gaps or holes in the UV coverage and with proper weighting of the data a very smooth effective distribution can be produced that accurately matches the idealized distribution everywhere. This would produce a PSF with negligible sidelobes and direct Fourier transform imaging can be used. This approach will produce high fidelity and dynamic range images without the application of special imaging techniques.

Weighting of the UV samples to produce a smoother distribution or to apply an edge taper to the UV coverage comes at the cost of decreased point source sensitivity. The paper by Boone presents an algorithm for building arrays that give complete coverage while approaching a Gaussian UV distribution [11]. Boone also quantifies the tradeoff between array size, sidelobe level and sensitivity loss associated with weighting the data to give a smooth bell shaped UV distribution. As the array magnification increases the array configurations become more ring-like and eventually circular. A 5-fold symmetric circular array of 64 antennas can achieve nearly complete coverage at a magnification of ~400 [12].

The discussion of complete UV coverage carries over to incomplete but uniform coverage for observations of regions where the sky brightness is confined to an area smaller than the angular resolution corresponding to the typical separation of the UV samples. Keto describes a method for constructing such uniform coverage configurations based upon Reuleaux triangles [13].

VI. DISCUSSION AND SUMMARY

The basic result here is that the near-in sidelobes are determined by the large-scale distribution of antennas, while the far sidelobes depend mostly upon the number of antennas and array magnification, assuming the configuration is suitably randomized. For magnifications larger than N, where N is the number of antennas, the standard deviation of the far sidelobes is $\sigma_D \approx 1/N$ and if the antennas are placed pseudo-randomly the distribution of the sidelobe amplitudes is $g(s) = N \exp(-Ns)$ and the peak sidelobe should be $s_{max} \approx 2/N \ln(mag)$. Placement of the antennas with a detectable pattern is likely to worsen the PSF while

optimization might improve both the distribution and the peak sidelobe level.

The expected standard deviation for the sidelobes is proportional to the magnification for magnifications less than N, $\sigma_D \propto mag$, and also decreases significantly when earth rotation synthesis is applied.

Applying an edge taper to the UV can improve the near-in sidelobes at the cost of a loss of sensitivity. The far sidelobes can be improved by weighting of the data to produce a smooth distribution if the fractional UV coverage exceeds unity over most of the UV plane of interest, again at the cost of losing point source sensitivity. But there is not much that can be done to improve the far sidelobes for snapshot images obtained with the highest magnification sparse configurations.

In general it is reasonable to select a large-scale distribution with near-in sidelobes that are at least as small as the far sidelobes to give the highest quality images without having to weight the data and suffer the associated loss in sensitivity. Thus filled or even centrally condensed array configurations are more appropriate for large arrays such as ALMA while arrays with a small number of antennas operating in snapshot mode would favor ring-like configurations, as has been pointed out by Holdaway [3].

Large arrays of 50 or more antennas require centrally condensed or bell shaped antenna distributions to keep the near-in sidelobes below the average far sidelobes. The standard deviation of the far sidelobes also decrease below 1/N as the array magnification drops below N or when earth rotation synthesis is used, further supporting the use of bell shaped antenna distributions. Earth rotation synthesis can also significantly reduce the far sidelobes for sparse arrays and hence even very small arrays may benefit from using bell shaped distributions.

A case for large arrays having complete UV coverage at the highest practical magnification (and therefore nearly uniform UV coverage) can be made for observation of very bright and complex sources. Appropriate tapering and weighting of the UV data can produce nearly perfect images from complete UV coverage data while suffering some loss in sensitivity. Unfortunately, given the current and projected array sensitivities at millimeter and sub-millimeter wavelengths, there are only a small number of sources bright enough to benefit from this approach.

The formulas in this paper can aid in making the tradeoff between the size and number of antennas during the initial conceptual design of an interferometer array. Equations 12, 16, 20 and 22 give a pretty complete picture of PSF sidelobe statistics and hence of the image quality as a function of the number of antennas. These equations quantify the improved image quality that an array of many small antennas will produce over an array of fewer larger antennas with the same total collecting area.

The results obtained are very general and can serve as a basis for developing configuration strategies. The statistics of the PSF for an actual or proposed configuration can be compared against the above formulas to determine whether it performs better or worse than a pseudo-random array. A companion paper will present the results for a few different arrays and demonstrate the accuracy and utility of the results given in this paper. The optimal configuration will depend upon the science goals for an array but the concepts and results derived here should make it easier to investigate the many options.

REFERENCES

[1]   J. W. Hardy, **Adaptive Optics for Astronomical Telescopes**, Oxford University Press, 1998, p. 116.
[2]   A.R. Thompson, J. M. Moran, and G. W. Swenson, **Interferometry and Synthesis in Radio** Astronomy, John Wiley and Sons, 1986.
[3]   M. Holdaway, "Comments on Minimum Sidelobe Configurations," MMA Memo 172, May 7, 1997.
[4]   Ref [1] p. 109.
[5]   Thompson, Moran and Swenson "Radio Interferometery"
[6]   L. Kogan, "Level of Negative Sidelobes in an Array Beam," Pub. Astron. Soc. Pac. vol. 111, pp. 510-511, 1999.
[7]   Ref. [2] p. 165.
[8]   J. Bass, **Principal of Probability**, p. 230.
[9]   Ref [2] p. 265.
[10] L. Kogan, "Optimizing a Large Array Configuration to Minimize the Sidelobe," IEEE Trans. Antennas Propagat., vol. 48, pp. 1075-1078, July 2000.
[11] F. Boone, "Interferometric array design: antenna positions optimized for ideal distributions of visibilities," Aston. & Astrophy, Feb. 2001.
[12] D. Woody, "ALMA Configurations with complete UV coverage," MMA memo #270, July 1999.
[13] E. Keto, "The Shapes of Cross-Correlation Interferometers," Ap. J. vol. 475, pp. 843-852, Feb. 1997.

The PSF of several sample arrays, including pseudo-random and circular arrays, are evaluated. The distribution of sidelobes is shown to closely follow the theoretical distribution derived in the companion paper [1]. An optimization procedure is developed that produces configurations with peak sidelobes close to the expected limit given in [1] and with a smooth progression from small peaks near the center of the PSF and the largest peaks at the edge of the primary beam. A radio interferometer [8] consists of a collection of spatially separated antennas. The aperture plane of the interferometer is the plane perpendicular to the instantaneous direction from the array to a reference point on the sky s0 called the phase-reference center. A baseline bij is dened as the vector between the 3D locations of two antennas i and j, projected onto this aperture plane. The components of bij are measured in units of wavelength Î» and denoted as u, v, w where u, v are 2D spatial frequencies and w describes the height of an antenna relative to the plane of the array in the dir...Â erogeneous antenna arrays corresponds to case where Gdijdâ€ Gdijd is not the same for all i and j. This is discussed in section IV-C. A. Correction for the W-term. Radio Interferometry has had a tremendous impact on the development of astrometry and geodesy. Barry Clark has played a leading role in developing the technology of radio interferometry through his work on connected-element interferometry, i.e., the Green Bank Interferometer and Very Large Array; and VLBI, i.e., the Mark I and II VLBI systems and the Very Long Baseline Array (VLBA). These efforts ... an interferometer array measures the Fourier transform of one. â€œcommonâ€ sky. Instead, in the presence of DDEs, each baseÂ â€“ Each observed visibility Vpq is a measurement of the sky coherency function X(u) at point upq, corrupted by some combination of multiplicative (per-antenna or per-interferometer) gain terms. â€“ The coherency function X(u) is a Fourier transform of the apparent sky Bapp(l) (see also Eq. (2)). The point spread function (PSF) describes the response of an imaging system to a point source or point object. A more general term for the PSF is a system's impulse response, the PSF being the impulse response of a focused optical system. The PSF in many contexts can be thought of as the extended blob in an image that represents a single point object. In functional terms, it is the spatial domain version of the optical transfer function of the imaging system. It is a useful concept in Fourier optics...